

Active Control of Flow Separation Over an Airfoil Using Synthetic Jets

Donghyun YOU, Parviz MOIN

Center for Turbulence Research, Stanford University, 488 Escondido Mall, Building 500, Stanford, California 94305, USA

Abstract. We perform large-eddy simulation of turbulent flow separation over an airfoil and evaluate the effectiveness of synthetic jets as a separation control technique. The flow configuration consists of flow over a NACA 0015 airfoil at Reynolds number of 896,000 based on the airfoil chord length and freestream velocity. A small slot across the entire span connected to a cavity inside the airfoil is employed to produce oscillatory synthetic jets. Detailed flow structures inside the synthetic-jet actuator and the synthetic jet/cross-flow interaction are simulated using an unstructured-grid finite-volume large-eddy simulation solver. Simulation results are compared with the experimental data of Gilarranz *et al.* [J. Fluids Eng. **127**, pp. 377-387 (2005)], and qualitative and quantitative agreements are obtained for both uncontrolled and controlled cases. As in the experiment, the present large-eddy simulation confirms that synthetic-jet actuation effectively delays the onset of flow separation and causes a significant increase in the lift coefficient. Modification of the blade boundary layer due to oscillatory blowing and suction and its role in separation control is discussed.

Key words: flow separation, synthetic jets, flow control, large eddy simulation (LES), airfoil.

1. Introduction

The performance of an airplane wing has a significant impact on the runway distance, approach speed, climb rate, payload capacity, and operation range, but also on the community noise and emission level as an efficient lift system also reduces thrust requirements (e.g., Ref. [12]). The performance of an airplane wing is often degraded by flow separation. Flow separation on an airfoil surface is related to the aerodynamic design of the airfoil profile. However, non-aerodynamic constraints such as material property, manufacturability, and stealth capability in military applications often conflict with the aerodynamic constraints, and either passive or active flow control is required to overcome the difficulty. Passive control devices, for example, vortex generators [5], have proven to be quite effective in delaying flow separation under some conditions. However, they can introduce a drag penalty when the flow does not separate. Over the past several decades various active flow control concepts have been proposed and evaluated to improve the efficiency and stability of lift systems by controlling flow separation. Many of these techniques involve continuous blowing or suction, which can produce effective control but is difficult to apply in real applications.

In recent years, control devices involving zero-net-mass-flux oscillatory jets or synthetic jets have shown good feasibility for industrial applications and effectiveness in controlling flow separation (e.g., Refs. [3, 10, 13]). The application of synthetic jets

to flow separation control is based on their ability to stabilize the boundary layer by adding/removing momentum to/from the boundary layer with the formation of vortical structures. The vortical structures in turn promote boundary layer mixing and hence momentum exchange between the outer and inner parts of the boundary layer. The control performance of the synthetic jets greatly relies on parameters such as the amplitude, frequency, and location of the actuation. Therefore an extensive parametric study is necessary for optimizing the control parameters.

For numerical simulations, an accurate prediction, not to mention control, of the flow over an airfoil at a practical Reynolds number is a challenging task. The flow over an airfoil is inherently complex and exhibits a variety of physical phenomena including strong pressure gradients, flow separation, and confluence of boundary layers and wakes (e.g., Refs. [7, 6, 14, 9]). The complex unsteady flow is difficult to compute by traditional computational fluid dynamics (CFD) techniques based on Reynolds-Averaged Navier-Stokes (RANS) equations [11]. For prediction of such unsteady flows, large-eddy simulation (LES) offers the best promise in the foreseeable future because it provides detailed spatial and temporal information regarding a wide range of turbulence scales, which is precisely what is needed to gain better insight into the flow physics of this configuration.

Recently, Gilarranz *et al.* [2] performed an experimental study of flow separation over a NACA 0015 airfoil with synthetic jet control. They reported the flow visualization, mean pressure coefficients, and wake profiles in both controlled and uncontrolled cases. However, the mechanism for separation control and how the boundary layer is modified by the control have not been clearly identified. In the present study we address the issues using large-eddy simulation. An understanding of the control mechanisms is valuable in reducing the effort for optimizing the control parameters. In this study we employ an unstructured-grid LES solver, CDP, to predict turbulent flow separation over an airfoil and its control by synthetic jets, and to understand the control mechanism for separation control. The unstructured-grid capability of the solver allows us to effectively handle the complex flow configuration involving an embedded synthetic-jet actuator and wind-tunnel walls. The present LES results are compared to the experimental data [2] in both controlled and uncontrolled cases. The effects of flow control on the boundary layer properties, flow separation, and lift enhancement are discussed.

2. Computational Methodology

2.1. NUMERICAL METHOD

The numerical algorithm and solution methods are described in detail in Refs. [8] and [4]; the main features of the methodology are summarized here. The spatially filtered incompressible Navier-Stokes equations for resolved scales in LES are

$$\frac{\partial \bar{u}_i}{\partial t} + \frac{\partial}{\partial x_j} \bar{u}_i \bar{u}_j = -\frac{\partial \bar{p}}{\partial x_i} + \frac{1}{\text{Re}} \frac{\partial}{\partial x_j} \frac{\partial \bar{u}_i}{\partial x_j} - \frac{\partial \tau_{ij}}{\partial x_j}, \quad (1)$$

$$\frac{\partial \bar{u}_i}{\partial x_i} = 0, \quad (2)$$

where τ_{ij} is the subgrid-scale (SGS) stress tensor modeled by the dynamic Smagorinsky closure [1]. All the coordinate variables, velocity components, and pressure are

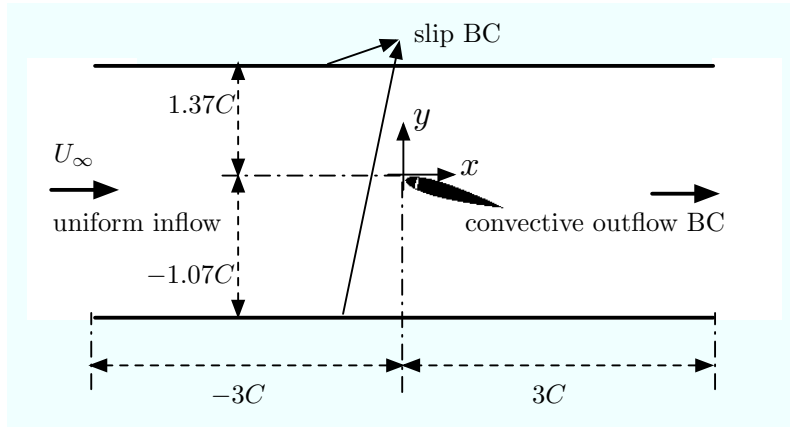


Figure 1. Flow configuration for LES of flow over a NACA 0015 airfoil with synthetic-jet control.

non-dimensionalized by the airfoil chord length C , the inflow freestream velocity U_∞ , and ρU_∞^2 , respectively. The time is normalized by C/U_∞ . The Cartesian velocity components and pressure are stored at the center of the computational elements. A numerical method that emphasizes discrete energy conservation was developed for the above equations on unstructured grids with hybrid, arbitrary elements. Controlling aliasing errors using kinetic energy conservation instead of employing numerical dissipation or filtering has been shown to provide good predictive capability for successful LES [15].

The temporal integration method used to solve the governing equations is based on a fully-implicit fractional-step method that avoids the severe time-step restriction that would occur in the synthetic jet orifice region with an explicit scheme. All terms in (1) and (2) are advanced using a second-order accurate fully-implicit method in time, and are discretized by the second-order central difference in space. A bi-conjugate gradient stabilized method (BCGSTAB) is used to solve the discretized nonlinear equations. The Poisson equation is solved by an algebraic multigrid method.

2.2. FLOW CONFIGURATION

The flow configuration is shown in figure 1. This configuration was experimentally studied by a team at Texas A&M [2]. In the experiment, a NACA 0015 airfoil with a chord length of 375mm was installed in a wind tunnel. The slot of the actuator had a width of 2mm across the entire length of the span and was placed at 12% of the chord measured from the leading edge on the suction side of the airfoil. This location was selected to provide sufficient volume to accommodate the synthetic-jet actuator inside the airfoil.

Figure 2 shows the maximum lift coefficient measured in the experiment [2] as a function of angle of attack (α) in both the uncontrolled and controlled cases. The use of the synthetic-jet actuator causes a dramatic increase in the maximum lift coefficient when the baseline (uncontrolled) flow separates. In the experiment, it was found that the angle of attack for which stall occurs is increased from 12° for an uncontrolled airfoil to approximately 18° for the controlled case. For the synthetic-jet actuation, the frequency of the actuation in the range of $60 \sim 130\text{Hz}$

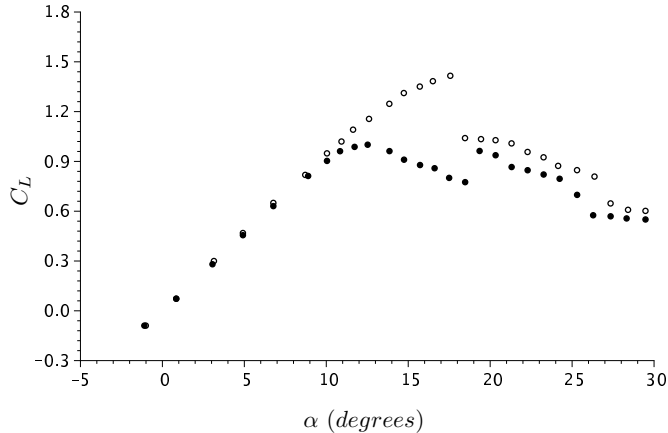


Figure 2. Lift coefficient as a function of angle of attack (α) measured by Gilarranz *et al.* [2]. \circ , controlled case ($f = 1.2U_\infty/C$); \bullet , uncontrolled case.

(or $fC/U_\infty = 0.65 \sim 1.40$) does not seem to have a significant effect on the maximum lift coefficient. Figure 2 indicates that the uncontrolled airfoil first suffers from a docile stall, which is also referred to as a trailing-edge stall when the angle of attack reaches approximately 12° . The separation point gradually moves upstream as the angle of attack increases. The leading-edge stall at approximately 19° produces an abrupt change in the lift coefficient. With the synthetic-jet actuation, the docile stall is effectively controlled and produces further enhanced lift coefficient up to the attack angle of approximately 18° . For an angle of attack greater than 18° , the controlled airfoil also suffers from a sharp drop of the lift coefficient due to the leading-edge stall, which is characterized by the formation of a separation bubble near the leading edge. Even after the massive stall (leading-edge stall) occurs, the synthetic-jet actuation increases the maximum lift coefficient compared to the uncontrolled case, but the amount of the lift augmentation is relatively small.

The present study focuses on cases with the angle of attack of 16.6° , where flow separates from the mid-chord location of the airfoil in the uncontrolled case, and the control effect is most remarkable. For this angle of attack, experimental data such as the mean surface pressure coefficients and wake profiles are available for comparison [2]. The computational domain is of size $L_x \times L_y \times L_z = 6C \times 2.44C \times 0.2C$. In the present LES, a smaller domain size than that in the experiment is employed in the spanwise direction to reduce the computational cost. The Reynolds number of this flow is 8.96×10^5 , based on the airfoil chord and inflow freestream velocity. In this study, it is important to precisely predict the flow through the synthetic-jet actuator because the directional variation of the jets during the oscillatory period greatly affects the boundary layer. Therefore, in the present study, the flow inside the actuator and resulting synthetic jets are simulated along with the external flowfield using an unstructured-grid capability of the present LES solver. Figure 3a shows the synthetic-jet actuator modeled with an unstructured mesh. In the experiment, a piston engine is utilized to generate a sinusoidal mass flux and generates synthetic jets through the spanwise cavity slot. To mimic the oscillatory motion of a piston engine in the experiment, we apply sinusoidal velocity boundary conditions to a cavity side wall as shown in figure 3b. Figure 3b shows the spanwise

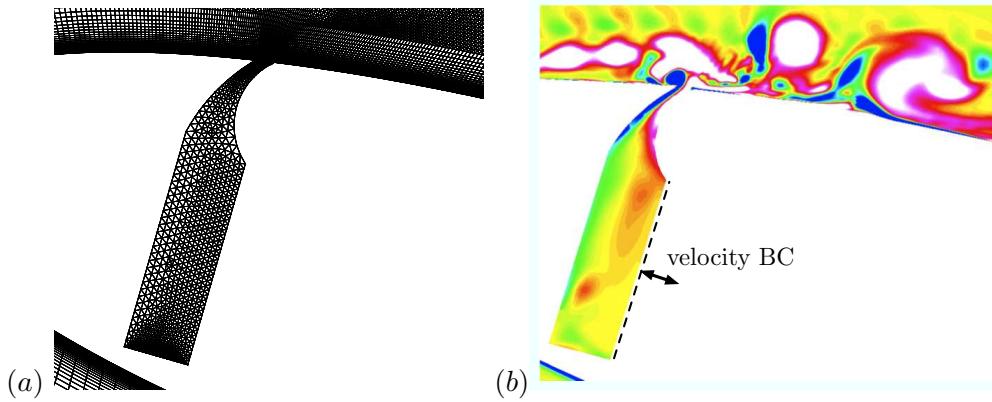


Figure 3. (a) Computational mesh and (b) instantaneous spanwise vorticity contours inside and around the synthetic-jet actuator. 20 contour levels in the range of $-50 \sim 60$ are shown.

vorticity contours representing flow inside the cavity and the interaction between synthetic jets and boundary layer flow. The frequency of the sinusoidal oscillation of the cavity side wall is $f = 1.284U_\infty/C$, which corresponds to 120Hz in the experiment of Gilarranz *et al.* [2]; the peak bulk jet velocity at the cavity exit nozzle is $U_{max} = 2.14U_\infty$. The same momentum coefficient as in the experiment is produced as:

$$C_\mu = \frac{h(\rho U_{max}^2)}{C(\rho U_\infty^2)} = 1.23 \times 10^{-2}, \quad (3)$$

where h is the width of the cavity nozzle exit. No-stress boundary conditions are applied along the top and bottom of the wind tunnel, and no-slip boundary conditions are applied on the airfoil surface and cavity wall. Periodic boundary conditions are used along the spanwise (z) direction. At the exit boundary, the convective boundary condition is applied, with the convection speed determined by the streamwise velocity averaged across the exit plane.

Two different mesh sizes of approximately 8 and 15 million cells have been employed while the results obtained with 8 million cells are presented in this paper. A total of 24 mesh points are allocated along the cavity slot. The grid spacings are distributed such that the resolution in the streamwise, wall-normal, and spanwise directions is less than 60, 1.2 and 16.2 wall-units, respectively. The simulation is advanced in time with a maximum Courant-Friedrichs-Lewy (CFL) number equal to 3.5, which corresponds to $\Delta t U_\infty / C \approx 1.7 \times 10^{-4}$, and each time step requires a wallclock time of approximately 15 seconds when 128 CPUs of the ASC Linux Cluster (2.4GHz Intel Pentium 4 Prestonia) are used. The present results are obtained by integrating the governing equations over an interval of approximately $20C/U_\infty$.

3. Results and Discussion

Gross features of the flow over uncontrolled and controlled airfoils are revealed in figure 4, showing iso-surfaces of the instantaneous vorticity magnitude overlapped with pressure contours predicted by the present LES. The vortical structures present

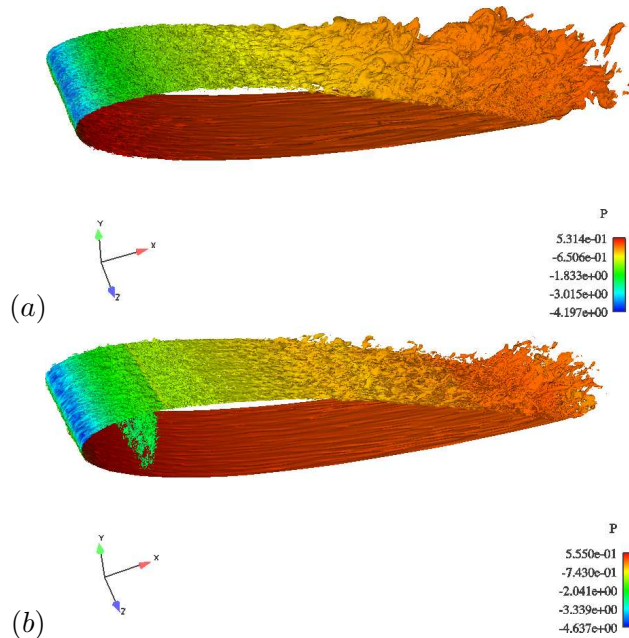


Figure 4. Iso-surfaces of the instantaneous vorticity magnitude ($|\Omega|C/U_\infty$) of 40 overlapped with the pressure contours. (a) Uncontrolled case; (b) controlled case.

Case	Uncontrolled		Controlled	
	C_L	C_D	C_L	C_D
Present LES	0.83	0.28	1.43	0.23
Experiment [2]	0.82	0.26	1.41	0.22

Table 1. Summary of lift and drag coefficients.

over the suction surface qualitatively indicate the degree of flow separation. In the uncontrolled case (figure 4a), flow massively separates from the half aft portion of the suction surface while the flow separation is dramatically prevented with the synthetic-jet actuation in the controlled case (figure 4b). Qualitatively, these features are consistent with the change in the experimentally measured maximum lift coefficient [2] with flow control (see figure 2).

The pressure distributions over the airfoil surfaces in both uncontrolled and controlled cases are compared with the experimental data in figure 5. In general, the present LES shows favorable agreement with experimental measurements in both cases. The pressure distribution directly indicates the effect of synthetic jets on flow separation. As seen in figure 5, most of the lift enhancement is achieved in the upstream portion of the airfoil suction surface, while the control effect of synthetic jets on the pressure distribution in the pressure surface is negligible.

The lift and drag coefficients predicted by the present LES in the uncontrolled and controlled cases are in excellent agreement with the experimental data [2] as shown in table 1. The present synthetic-jet actuation with the momentum coefficient of 1.23% produces more than a 70% increase in the lift coefficient. The drag coefficient is found to decrease approximately 15% ~ 18% with the synthetic-jet actuation.

The drag reduction due to the synthetic-jet actuation is also indicated by the wake

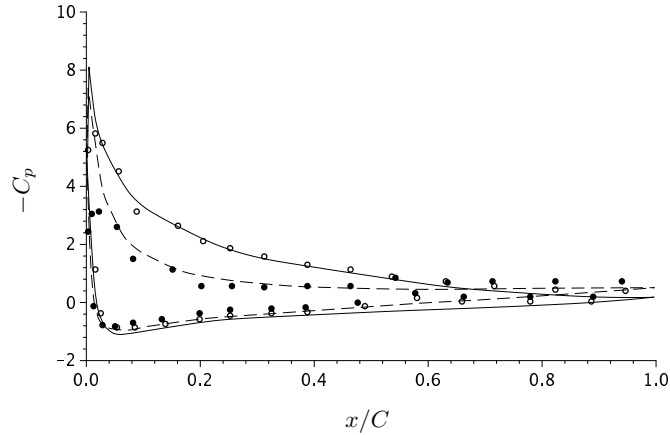


Figure 5. Mean pressure distribution over the airfoil surface. Solid line, controlled case; dashed line, uncontrolled case; symbols, experimental data [2].

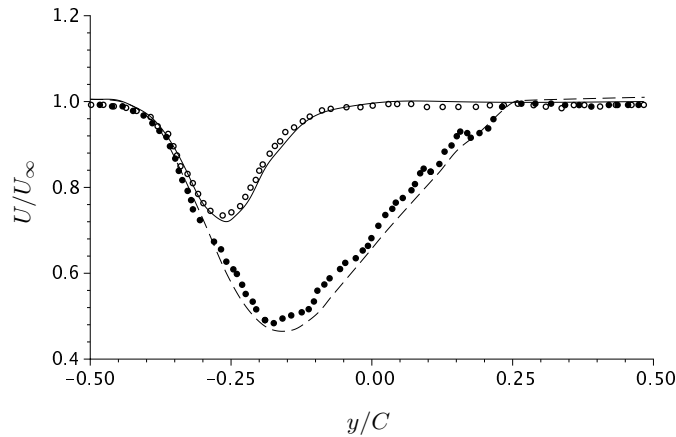


Figure 6. Mean streamwise velocity profiles at $x/C = 1.2$. Solid line, controlled case; dashed line, uncontrolled case; symbols, experimental data [2].

profiles. Figure 6 shows the mean streamwise velocity profiles in the uncontrolled (----) and controlled (—) cases in a downstream location at $x/C = 1.2$. The width of the wake and the peak magnitude of velocity deficit decrease with synthetic jet control. The present wake profiles are in favorable agreement with experimental data [2] in both uncontrolled and controlled cases.

Both the suction and blowing phases modify the boundary layer on the suction surface of the airfoil. The synthetic-jet actuation not only stabilizes the boundary layer either by adding/removing the momentum to/from the boundary layer, but also enhances mixing between inner and outer parts of the boundary layer. The change of the blade boundary layer during a period of synthetic-jet actuation is shown in figure 7 in terms of the phase-averaged streamlines. In the suction phase (figure 7a) the low momentum flow in the upstream boundary layer is removed by the suction and prevents downstream flow separation. On the other hand, synthetic-jet blowing (figure 7c) energizes the downstream boundary layer and prevents downstream flow

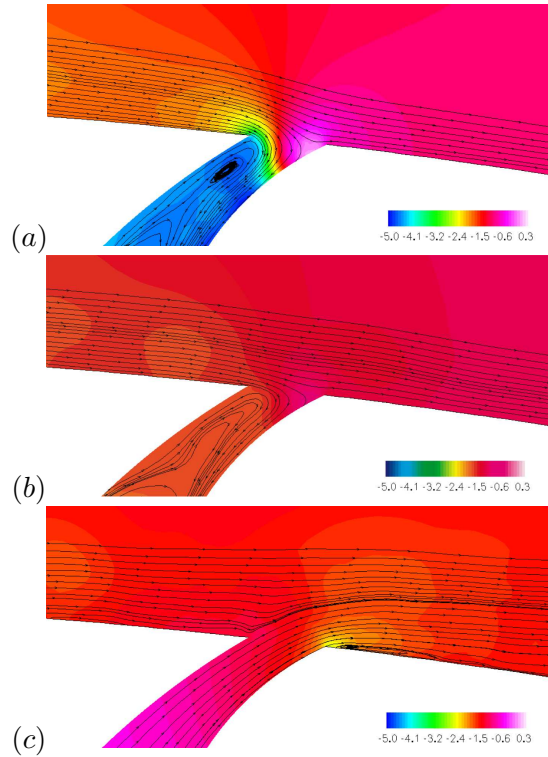


Figure 7. Mean streamlines overlapped by the mean pressure contours. (a) $(1/4)T$ (suction phase); (b) $(2/4)T$; (c) $(3/4)T$ (blowing phase), where T denotes the period of synthetic-jet actuation.

separation. The modification of the boundary layer in the upstream ($x/C = 0.11$) and downstream ($x/C = 0.16$) proximity to the exit slot of the synthetic-jet actuator ($x/C = 0.12$) is shown in figure 8. Compared to the velocity profile in the uncontrolled case (\circ), in the blowing phase (Fig. 8a), the downstream velocity profile becomes fuller due to additional momentum while the modification of the upstream velocity profile is not noticeable. On the other hand, in the suction phase (Fig. 8b), the thickness of the downstream boundary layer is significantly thinned. Therefore, the downstream flow separation is effectively prevented by the favorable modification of the blade boundary layer in both the blowing and suction phases.

4. Conclusions

We have performed large-eddy simulation of turbulent flow separation over an airfoil with synthetic-jet control. Detailed flow structures inside a synthetic-jet actuator and the synthetic jet/cross-flow interaction have been simulated using an unstructured-grid finite-volume large-eddy simulation solver. Simulation results show favorable agreements with experimental data in terms of mean pressure coefficients and wake profiles for both uncontrolled and controlled cases. For a docile stall, synthetic-jet actuation has been found to stabilize the blade boundary layer and effectively delay the onset of flow separation and cause a significant increase in the lift coefficient.

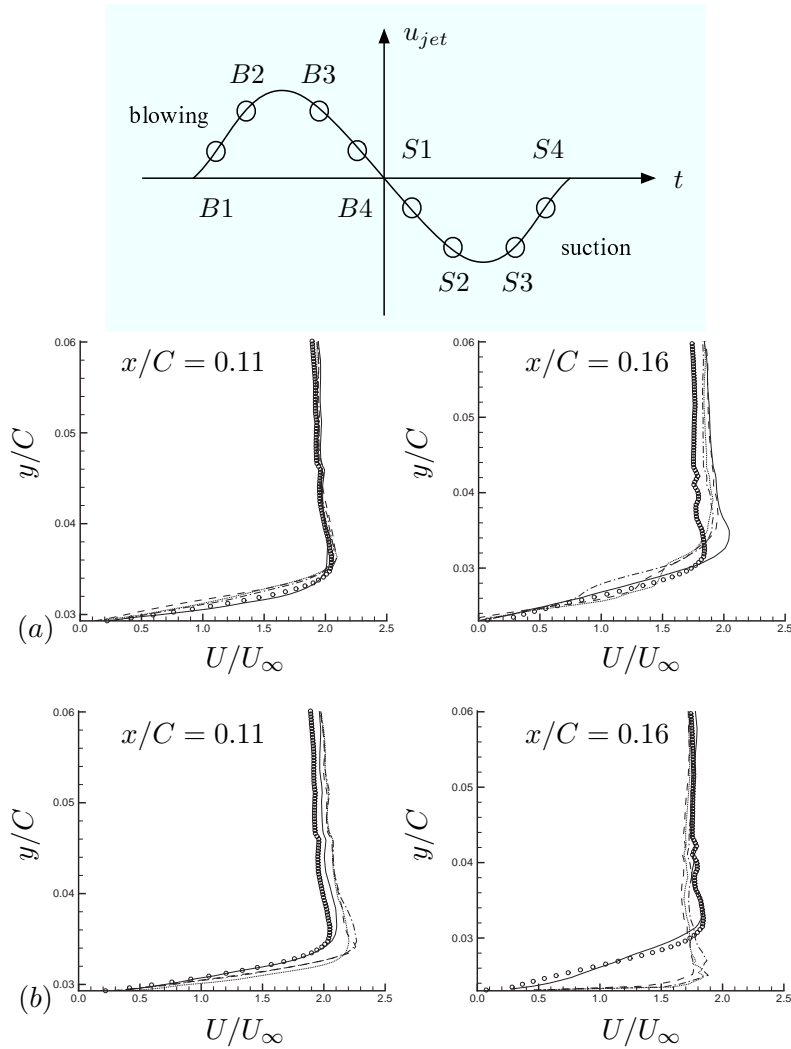


Figure 8. Profiles of the phase-averaged streamwise velocity. (a) blowing phase: —, B1; ----, B2; ·····, B3; —·—, B4; (b) suction phase: —, S1; ----, S2; ·····, S3; —·—, S4. \circ , uncontrolled case. The cavity slot is located at $x/C = 0.12$.

Acknowledgements

The authors gratefully acknowledge support from Boeing company and valuable discussions with Dr. Arvin Shmilovich. The authors are also grateful to Dr. Frank Ham for his help with the unstructured LES solver CDP.

References

- [1] M. Germano, Ugo Piomelli, Parviz Moin, and W. H. Cabot. A dynamic subgrid-scale eddy-viscosity model. *Physics of Fluids (A)*, 3(7):1760–1765, 1991.
- [2] J. L. Gilarranz, L. W. Traub, and O. K. Rediniotis. A new class of synthetic jet actuators - part II: application to flow separation control. *Journal of Fluids Engineering*, 127:377–387, 2005.

- [3] Ari Glezer and Michael Amitay. Synthetic jets. *Annual Review of Fluid Mechanics*, 34:503–529, 2002.
- [4] F. Ham and G. Iaccarino. Energy conservation in collocated discretization schemes on unstructured meshes. Annual Research Briefs, 3-14, Center for Turbulence Research, Stanford, California, 2004.
- [5] A. Jirasek. A vortex generator model and its application to flow control. *AIAA Paper 2004-4965*, 2004.
- [6] M. R. Khorrami, M. E. Berkman, and M. Choudhari. Unsteady flow computations of a slat with blunt trailing edge. *AIAA Journal*, 38(11):2050–2058, 2000.
- [7] M. R. Khorrami, B. A. Singer, and R. H. Radeztsky. Reynolds-averaged navier-stokes computations of a flap-side-edge flowfield. *AIAA Journal*, 37(1):14–22, 1999.
- [8] K. Mahesh, G. Constantinescu, S. Apte, G. Iaccarino, F. Ham, and P. Moin. Large-eddy simulation of reacting turbulent flows in complex geometries. *Journal of Applied Mechanics*, 73:374–381, 2006.
- [9] D. L. Mathias, K. R. Roth, J. C. Ross, S. E. Rogers, and R. M. Cummings. Navier-Stokes analysis of the flow about a flap edge. *Journal of aircraft*, 36(6):833–838, 1999.
- [10] C. L. Rumsey, T. B. Gatski, W. L. Sellers III, V. N. Vatsa, and S. A. Viken. Summary of the 2004 CFD validation workshop on synthetic jets and turbulent separation control. *AIAA Paper 2004-2217*, June 2004.
- [11] C. L. Rumsey and S. X. Ying. Prediction of high lift: Review of present CFD capability. *Progress in Aerospace Sciences*, 38:145–180, 2002.
- [12] J. J. Thibert, J. Reneaux, F. Moens, and J. Priest. ONERA activities on high lift devices for transport aircraft. *Aeronautical Journal*, 99:395–411, 1995.
- [13] I. Wygnanski. The variables affecting the control of separation by periodic excitation. *AIAA Paper 2004-2505*, 2004.
- [14] S. X. Ying, F. W. Spaid, C. B. McGinley, and C. L. Rumsey. Investigation of confluent boundary layers in high-lift flows. *Journal of aircraft*, 35(3):550–562, 1998.
- [15] D. You, M. Wang, and P. Moin. Large-eddy simulations of flow over a wall-mounted hump with separation control. *AIAA Journal*, 44(11):2571–2577, 2006.